Dynamic Article Links ▶

PAPER

Fluorescent magnetic nanoparticles for biomedical applications

Nataliya Chekina,[a] Daniel Horák,*[ab] Pavla Jendelová,[bc] Miroslava Trchová,[a] Milan J. Beneš,[a] Martin Hrubý,[a] Vít Herynek,[bd] Karolina Turnovcová[c] and Eva Syková[bc]

The simultaneous combination of optical and magnetic resonance imaging (MRI) would greatly benefit *in vivo* disease diagnosis as well as *in situ* monitoring of living cells. In order to design dual detection of cells involving simultaneous imaging by fluorescent microscopy and MRI, nanoparticles with two reporters, a fluorescent dye and a superparamagnetic core, included in one particle were synthesized and characterized. The $\gamma\text{-Fe}_2\text{O}_3$ nanoparticles obtained by coprecipitation and oxidation were coated with silica (SiO_2) or carboxymethyl chitosan (CMCS) and labeled with fluorescein isothiocyanate (FITC). The fluorescent label was covalently bound to the nanoparticles and was not quenched by the iron oxide core. The nanoparticles successfully labeled rat mesenchymal stem cells (rMSCs) *in vitro*. Relaxation time measurements found large amounts of iron inside the cells with FITC-labeled $\gamma\text{-Fe}_2\text{O}_3\text{–SiO}_2\text{-AP}$ nanoparticles. Both MR and fluorescent imaging of a rat brain with implanted rMSCs labeled with FITC-labeled CMCS-modified silica-coated $\gamma\text{-Fe}_2\text{O}_3$ nanoparticles were performed.

1. Introduction

Magnetic nanoparticles play an increasingly important role in science and technology.[1,2] Since they are nontoxic and biodegradable, they are widely used in biology and medicine for imaging,[3,4] cell tracking,[5] drug and siRNA delivery,[6,7] hyperthermia,[8,9] magnetic separation[10,11] and bio- and chemo-sensoring.[12] To improve the efficiency and versatility of nanomaterials in numerous applications, hybrid magnetic nanoparticles incorporating multiple functionalities are being developed. With regard to cell labeling, there is a focus on materials that possess both fluorescent and magnetic properties so that they can be monitored not only by MRI, but also by fluorescent spectroscopy.[13–23] Optical techniques offer improved high spatial resolution allowing the visualization of cell structures.[24] They are used for the simultaneous visualization of multiple modalities with two or more fluorescent probes with different spectra, but have limited depth of imaging and poor absolute quantitative accuracy due to the absorption of light in tissues. Magnetic imaging has no practical limitation in terms of the depth of imaging; however, spatial resolution is worse and imaging with more than one probe is problematic. A combination of multiple imaging technologies, such as magnetic and optical imaging, provides complementary information about the imaged object.

Fluorescent magnetic nanocomposites include a variety of materials based on a magnetic core coated with an inorganic compound or organic polymer with a bound or embedded[25] fluorophore (quantum dots,[26] organic dyes,[15] conjugated polymers, and Eu complexes[16,27]). Since quantum dots contain toxic elements such as cadmium or selenium, dye-conjugated magnetic particles are preferred for *in vivo* applications. The preparation of fluorescent magnetic nanoparticles is, however, challenging. Problems are also associated with their low chemical stability and the aggregation of the nanoparticles in solution. Aggregation is caused by magnetic, electrostatic, hydrophobic or chemical interactions between the particles. A specific difficulty in the preparation of fluorescent magnetic nanoparticles is the risk of quenching of the fluorophore on the particle surface by the magnetic core. This problem has been solved by coating the magnetic core with a stable isolating shell prior to the introduction of the fluorescent molecule or by attaching an appropriate spacer to the fluorophore. Most fluorescent magnetic nanoparticles thus have a core–shell structure.[15] The shell has to be biocompatible and non-immunogenic, preventing the agglomeration of the particles and at the same time minimizing non-specific interactions with proteins, cells and other components of biological media.

A convenient coating of magnetic cores is based on their silanization with tetraethoxysilane and/or its functional derivatives for binding a fluorophore.[28] The silica shell serves as an inert, biocompatible protective coating. Moreover, it improves the colloidal stability of particles in aqueous media, is easy to prepare and is optically transparent. A properly functionalized

[a] Institute of Macromolecular Chemistry, Academy of Sciences of the Czech Republic, Heyrovský Sq. 2, 162 06 Prague 6, Czech Republic. E-mail: horak@imc.cas.cz
[b] Center for Cell Therapy and Tissue Repair, Charles University, V Úvalu 84, 150 06 Prague 5, Czech Republic
[c] Institute of Experimental Medicine, Academy of Sciences of the Czech Republic, Vídeňská 1083, 142 20 Prague 4, Czech Republic
[d] Institute for Clinical and Experimental Medicine, Vídeňská 1958/9, 140 21 Prague 4, Czech Republic

silica shell has the ability to incorporate not only a fluorescent label, but also other functional molecules, such as biological species.[29,30] Sol–gel methods using tetraethoxysilane (TEOS) are generally used to produce coatings of controlled thickness.[31] Functional silanes, such as (3-aminopropyl)triethoxysilane (APTES), then allow the introduction of reactive groups to the core–shell structures. However, the non-degradability of the silica limits its *in vivo* biomedical use.[32]

Another alternative for the preparation of multimodal fluorescent magnetic nanoparticles involves coating the magnetic cores with polysaccharides, such as dextran, chitosan or their derivatives, followed by the attachment of a label. Due to its biocompatibility and biodegradability, chitosan (CS)[33–35] has been widely used in tissue engineering and controlled drug and gene delivery.[36,37] CS is blood compatible and enhances interactions with the cell membrane,[38] which may facilitate the uptake of carboxymethyl chitosan (CMCS)-coated magnetic nanoparticles by cells. CMCS has chelating groups (causing strong interactions with magnetic oxide and thus binding to it) and amphiphilic properties.[39] The carboxymethylation of chitosan enables its solubility in water at neutral and alkaline pH, allowing the introduction of additional functional groups for chemical bonding of fluorescent labels.[40]

The aim of this work was to design, prepare and characterize new dual-marker particles, simultaneously combining both fluorescent and magnetic properties in one entity. Such bimodal fluorescent/magnetic nanoparticles have potential applications in biotechnology and nanomedicine. As a fluorescent label, fluorescein isothiocyanate (FITC) has been chosen, as it allows facile labeling of various structures. FITC has often been used in laser-induced fluorescence detection techniques and flow cytometry for protein labeling[41,42] as well as imaging and separation of chiral amino acids.[43,44] The advantage of fluorescein is that its emission intensity is pH-dependent. Fluorescence strongly increases[45] in the pH range 5–8, where the fluorescent magnetic nanoparticles may serve as a "smart" pH-sensing fluorescent probe for functional imaging. In normal tissue and the bloodstream, the pH is 7.4 and the fluorescence intensity is high. In contrast, in tumors or inflamed tissue, which are slightly acidic (pH *ca.* 6.5) due to hypoxic conditions, fluorescence intensity is low; after internalization of the particles into cells, the pH drops even further to *ca.* 5 in late endosomes.[46] This offers a unique possibility to simultaneously follow both the biodistribution of the particles using magnetic resonance imaging (MRI) and the pH of the surrounding microenvironment of the nanoparticles, *e.g.*, in tumors or inflammatory lesions.

2. Experimental

2.1. Materials

Iron(II) chloride tetrahydrate and iron(III) chloride hexahydrate, (3-aminopropyl)triethoxysilane (APTES), 2-(*N*-morpholino)ethanesulfonic acid (MES), 1-ethyl-3-[3-(dimethylamino)propyl]carbodiimide (EDC), *N*-hydroxysulfosuccinimide (sulfo-NHS), fluorescein isothiocyanate (FITC) and phosphate buffer solution (PBS) were purchased from Sigma-Aldrich (St Louis, MO, USA). Ammonium hydroxide, sodium hydroxide, propan-2-ol and ethanol (99.8%) were obtained from Lach-Ner (Neratovice,

Czech Republic). Chitosan (CS; middle viscous), monochloroacetic acid and tetraethoxysilane (TEOS) were obtained from Fluka (Buchs, Switzerland); sodium citrate dihydrate was from Lachema (Brno, Czech Republic). The contrast agent Endorem® was from Guerbet (Roissy, France). All other chemicals were from Aldrich. Ultrapure Q-water ultrafiltered on a Milli-Q Gradient A10 system (Millipore, Molsheim, France) was used for the preparation of solutions.

2.2. Preparation of γ-Fe$_2$O$_3$ nanoparticles

Iron oxide nanoparticles were prepared by a modified method according to an earlier published procedure,[47] in which colloidal Fe(OH)$_3$ was precipitated from FeCl$_3$·6H$_2$O added to less than an equimolar amount of ammonia; this was followed by the addition of FeCl$_2$·4H$_2$O at a molar ratio Fe(III)/Fe(II) = 2. Briefly, 0.2 M FeCl$_3$·6H$_2$O aqueous solution (100 mL) was mixed with 0.5 M NH$_4$OH solution (100 mL) under sonication (Digital Sonifier 250; Branson Ultrasonics, Danbury, CT, USA) at 40 W and laboratory temperature for 5 min to form the Fe(OH)$_3$ colloid. Then, 0.2 M FeCl$_2$·4H$_2$O aqueous solution (50 mL) was added under sonication (5 min) and the mixture poured into 0.5 M NH$_4$OH aqueous solution (300 mL). The resulting magnetite coagulate was left to grow for 30 min, magnetically separated, and repeatedly (7 times) washed with Q-water to remove all impurities (including NH$_4$Cl) remaining after the synthesis. The above formed pure magnetite was sonicated for 5 min with 0.1 M sodium citrate solution (16 mL) and oxidized at room temperature with 5 wt% sodium hypochlorite (13 mL) to maghemite (γ-Fe$_2$O$_3$). The precipitate was again repeatedly (seven times) washed with Q-water using magnetic separation/decantation to obtain a stable colloid.

2.3. Synthesis of carboxymethyl chitosan (CMCS)

A slight modification of a previously described procedure was used for the preparation of carboxymethyl chitosan.[40,48] Briefly, CS (10 g) was swelled in propan-2-ol/water (80/20, v/v) mixture (100 mL), sodium hydroxide (15 g, 375 mmol) was added, and the reaction proceeded at 60 °C for 1 h. A solution of chloroacetic acid (15 g, 159 mmol) in propan-2-ol (20 mL) was added dropwise to the reaction mixture over 30 min, and the reaction proceeded at 60 °C for 4 h. The reaction was cooled, diluted by the addition of 95% ethanol (200 mL) and the NaCl precipitate was filtered-off. Water (500 mL) and 2.5 M HCl (5 mL) were then added to reach pH 7. Unreacted CS was removed after centrifugation (1000 rpm) for 10 min. The volume of the supernatant was reduced to 100 mL by evaporation under vacuum, and 99.8% ethanol (400 mL) was added to precipitate the CMCS. Finally, the CMCS was filtered, washed three times with 99.8% ethanol and dried in a vacuum oven at 50 °C.

2.4. Surface modification of γ-Fe$_2$O$_3$ nanoparticles

2.4.1. Preparation of γ-Fe$_2$O$_3$–SiO$_2$ nanoparticles. The above-prepared magnetic iron oxide nanoparticles were coated with silica according to an earlier report.[49] The γ-Fe$_2$O$_3$ nanoparticles (2 g) were dispersed in water (60 mL), the pH of the dispersion was adjusted to 11 by the addition of 25% ammonium hydroxide solution and a solution of TEOS (2.5 mL) in ethanol

This journal is © The Royal Society of Chemistry 2011

J. Mater. Chem., 2011, **21**, 7630–7639 | 7631

(25.5 mL) was added. The mixture was stirred for 18 h at 23 °C to hydrolyze the TEOS and to attach the silica on the iron oxide surface. The resulting γ-Fe$_2$O$_3$–SiO$_2$ nanoparticles were washed six times with Q-water using magnetic separation/decantation.

2.4.2. Preparation of γ-Fe$_2$O$_3$–SiO$_2$-AP nanoparticles. The silica-coated nanoparticles were dispersed in Q-water (100 mL), a solution of APTES (2.63 g, *i.e.*, 50 μmol per m^2 of the nanoparticle surface) in ethanol (100 mL) was added and the pH of the mixture was adjusted to 11 by several drops of 40 wt% KOH aqueous solution. The reaction mixture was then heated at 50 °C for 5 h under stirring (350 rpm). After cooling, the γ-Fe$_2$O$_3$–SiO$_2$-AP nanoparticles were washed six times with Q-water using magnetic separation/decantation to remove any unbound APTES from the dispersion.

2.5. Immobilization of CMCS on the surface of γ-Fe$_2$O$_3$ nanoparticles

2.5.1. Preparation of γ-Fe$_2$O$_3$–CMCS nanoparticles. To bind CMCS on the surface of γ-Fe$_2$O$_3$ nanoparticles, the nanoparticles (10 mg) were dispersed in an aqueous solution of CMCS (10 mL water; 0.2 mg CMCS per mL; pH 7.4) at room temperature for 12 h under stirring. The resulting γ-Fe$_2$O$_3$–CMCS nanoparticles were washed three times with Q-water using magnetic separation/decantation to remove any non-adsorbed CMCS from the dispersion.

2.5.2. Preparation of γ-Fe$_2$O$_3$–SiO$_2$-AP–CMCS nanoparticles. Alternatively, the γ-Fe$_2$O$_3$–SiO$_2$-AP nanoparticles (50 mg) were added to a solution of CMCS (25 mg), EDC (30 mg) and sulfo-NHS (10 mg) in 0.1 M MES buffer (10 mL; pH 6.5). The mixture was sonicated at 40 W and 4 °C for 10 min and shaken at room temperature for 24 h. The γ-Fe$_2$O$_3$–SiO$_2$-AP–CMCS nanoparticles were magnetically separated and washed with a MES buffer.

2.5.3. Preparation of fluorescent γ-Fe$_2$O$_3$ nanoparticles. FITC-labeled γ-Fe$_2$O$_3$ nanoparticles were prepared according to the method reported in the literature.[50] Briefly, a solution of FITC (3 mg) in an acetone/water mixture (0.3/2.7, v/v) was added to a dispersion of γ-Fe$_2$O$_3$–SiO$_2$-AP, γ-Fe$_2$O$_3$–CMCS or γ-Fe$_2$O$_3$–SiO$_2$-AP–CMCS nanoparticles (10 mg) in PBS (10 mL; pH 7.4). The reaction proceeded for 12 h at 23 °C in the dark. The FITC-labeled γ-Fe$_2$O$_3$ nanoparticles were magnetically separated and washed five times with PBS (pH 7.4) to remove non-conjugated FITC.

2.6. Characterization

Magnetic nanoparticles were observed in a Tecnai Spirit G^2 transmission electron microscope (TEM; FEI, Brno, Czech Republic). Size and polydispersity (PDI = D_w/D_n, where D_w and D_n are the weight- and number-average particle diameters, respectively) were determined from micrographs using Atlas image analysis software (Tescan, Brno, Czech Republic). The iron content in the microspheres was determined by atomic absorption spectroscopy (AAS, Perkin-Elmer 3110) of an extract from the sample obtained with dilute HCl (1 : 1) at 80 °C for 1 h.

The concentration of APTES on the surface of the iron oxide nanoparticles was determined by CHN elemental analysis.

A Thermo Nicolet NEXUS 870 FTIR Spectrometer (Madison, WI, USA) in an H$_2$O-purged environment with a DTGS detector was used to measure the infrared spectra over a wavelength range of 400 to 4000 cm^{-1}. A MKII Golden Gate™ Heated Diamond ATR Top-Plate (Specac, Orpington, Great Britain) was used to measure the spectra of powdered samples by reflection ATR spectroscopy. Typical parameters were 256 sample scans, resolution 4 cm^{-1}, Happ-Genzel apodization and KBr beamsplitter.

The fluorescence spectra of FITC-labeled γ-Fe$_2$O$_3$ nanoparticles were measured by a Jasco FP 6200 spectrofluorimeter (Jasco Analytical Instruments, Easton, MD, USA).

2.7. Cell experiments with fluorescent magnetic nanoparticles

2.7.1. Cell experiments. As a model for testing cell viability and labeling efficiency, rat mesenchymal stem cells (rMSCs) were used. The cells were isolated from rat femur bones as described elsewhere.[51] Cells from passages 2–4 were labeled by adding a suspension of FITC-labeled γ-Fe$_2$O$_3$–SiO$_2$-AP nanoparticles, FITC-labeled γ-Fe$_2$O$_3$–CMCS nanoparticles or FITC-labeled γ-Fe$_2$O$_3$–SiO$_2$-AP–CMCS nanoparticles at a concentration of 22 μg γ-Fe$_2$O$_3$ per mL to the cultivation media (DMEM, 10% fetal bovine serum and 2% Primocin) for 72 h. As a control, a commercial contrast agent, dextran-coated γ-Fe$_2$O$_3$ Endorem®, was used. At the end of the labeling experiment, the cells were harvested and counted in a Bürker chamber. Viability was determined using the trypan blue exclusion test, which determines the number of viable cells present in a cell suspension. The test is based on the principle that live cells possess intact cell membranes that exclude certain dyes, such as trypan blue, whereas dead cells do not.[52]

2.7.2. Labeling efficiency and staining intensity. Labeling efficiency was determined by manually counting the number of Prussian Blue-stained and unstained cells in 12-well plates. Ten optical fields from each well were scanned using an Axioplan Imaging II microscope at 100× magnification using a 10×/0.75 objective lens, an AxioCam digital camera and AxioVision 4 software (microscope setup from Zeiss, Oberkochen, Germany). All cells in the scanned images were manually labeled as Prussian Blue-stained or unstained using Jasc Paint Shop Pro 8 (Corel Corporation, Ottawa, Canada). The scanned images with manually labeled cells were processed by the Image analysis toolbox of MATLAB software (The MathWorks, MA, USA). The presence or absence of a label inside the cells was expressed as the percentage of labeled cells. To check the intensity of fluorescent staining, an Axioplan Imaging II fluorescent microscope was used at a magnification of 200×. Data were analyzed for statistical significance with analysis of variance (ANOVA) using the Origin program, version 8.0988 (OriginLab Co., Northampton, MA, USA).

2.8. *In vitro* MR relaxometry

T_2 relaxation times were measured at two fields: at 0.5 T using a Bruker MiniSpec relaxometer and at 4.7 T using a Bruker

BioSpec spectrometer (Etlingen, Germany). The relaxivities r_2 (reciprocal values of relaxation times related to the concentration c, *i.e.*, $1/T_2/c$) of the fluorescent magnetic particles dispersed in gelatin and the relaxation rates R_2 of the rMSCs (*i.e.*, $1/T_2$/cell number in 1 mL) labeled with such particles were calculated at both fields. The contribution of the gelatin and/or unlabeled cells was deducted.

The amount of iron inside the cells was evaluated by comparing the relaxivity of a sample with labeled cells to calibration samples containing pure contrast agent at known concentrations in gelatin. As this method does not reflect the possible aggregation of nanoparticles inside the cells, which may significantly alter relaxation times, the calculated average amount of iron inside the cells is underestimated and should be considered as a rough estimate only. As the nanoparticles are superparamagnetic, they exhibit strong T_2 and moderate T_1 effect (ratio $r_2/r_1 = 20.7 \pm 1.2$ at 0.5 T), and are dedicated primarily for contrast enhancement in T_2- (or T_2^*) weighted images. Due to strong T_2^* they are unsuitable for T_1-weighted imaging. Therefore, only r_2 relaxivities and R_2 relaxation rates are presented.

2.9. MR imaging

In vivo MR images of grafted labeled cells in the rat brain were obtained using a 4.7 T Bruker spectrometer equipped with a homemade surface coil. The rats were anesthetized by passive inhalation of 1.5–2% isoflorane in air. Breathing was monitored during the measurements. Single sagittal, coronal and transversal images were obtained by a fast gradient echo sequence for localizing the subsequent T_2-weighted turbo-spin echo sequence in the coronal and transversal planes. Sequence parameters were: repetition time TR = 3000 ms, effective echo time TE = 36 ms, number of acquisitions AC = 8, matrix size 256 × 256, field of view FOV = 3.5 × 3.5 cm, the slice thickness was 0.85 mm. All experiments with rats were performed in compliance with the relevant laws and institutional guidelines. The institutional committee has approved the experiments.

3. Results and discussion

3.1. Preparation of silica-coated γ-Fe₂O₃ nanoparticles

At the beginning, *ca.* 9 nm γ-Fe₂O₃ nanoparticles with a relatively narrow polydispersity (PDI = 1.25) were obtained by the chemical coprecipitation of Fe(II) and Fe(III) chloride with ammonium hydroxide and oxidation with sodium hypochlorite (Fig. 1(a)). The nanoparticles were stabilized using sodium citrate.

Two approaches for binding a fluorescent label on coated magnetic nanoparticles were used. The first one was two-step silanization by TEOS followed by APTES catalyzed by ammonium hydroxide[53,54] to introduce the amino groups necessary for ligand attachment (Scheme 1). In the second method, γ-Fe₂O₃ or γ-Fe₂O₃–SiO₂-AP nanoparticles were coated with CMCS and FITC immobilized. Silane was covalently attached to the iron oxide surface by the reaction between the hydroxyl groups of hydrolyzed TEOS and the hydroxyl groups on the γ-Fe₂O₃ surface. The resulting *ca.* 13 nm γ-Fe₂O₃ particles had a *ca.* 3 nm thick continuous silica shell on the surface (Fig. 1(b)). Coating
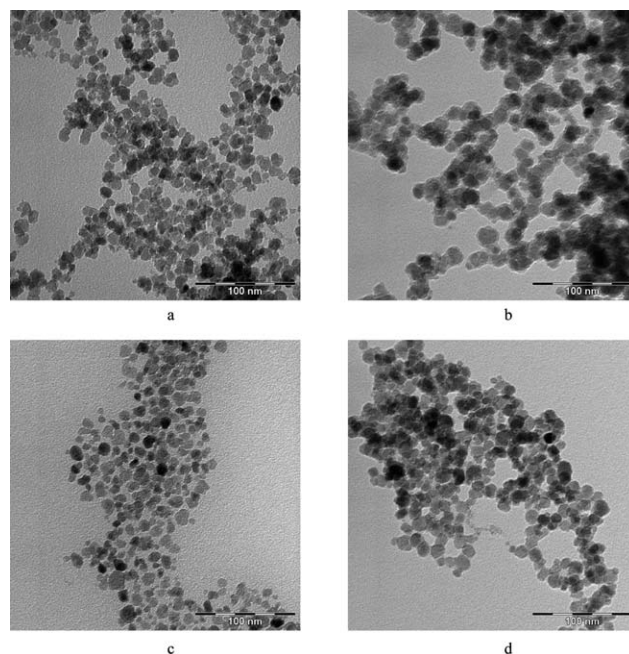

Fig. 1 TEM micrographs of (a) γ-F₂O₃ nanoparticles, (b) silica-coated γ-F₂O₃ nanoparticles, (c) γ-F₂O₃–CMCS nanoparticles and (d) γ-F₂O₃–SiO₂-AP–CMCS nanoparticles.

did not change the polydispersity of the nanoparticles (PDI = 1.14). Several factors, such as pH, temperature and APTES concentration in the feed, influence the efficiency of the modification. The surface charge of the nanoparticles is determined by the pH of the reaction mixture and by the selection of the catalyst for APTES hydrolysis. No amino groups were observed on the surface of the silica-coated γ-Fe₂O₃ nanoparticles at pH 3. APTES modification of silica-coated γ-Fe₂O₃ nanoparticles was thus performed under alkaline conditions (pH = 11) at 50 °C, which accelerated the reaction compared to room temperature. This is in accordance with claims in the literature that the optimal conditions for such a synthesis require alkaline catalysis.[49] The concentrations of APTES in the reaction feed were varied from 50 to 100 μmol m⁻² of silica-coated γ-Fe₂O₃ nanoparticles (Table 1). If 50 μmol of APTES per m² was added in the reaction feed, 3.6 μmol of APTES was found per m² of γ-Fe₂O₃ surface, corresponding to 2.2 APTES molecules per nm². Increasing the APTES concentration in the reaction feed up to 75 or 100 μmol m⁻² resulted in greater coverage of the silica-coated γ-Fe₂O₃ nanoparticle surface with APTES, up to 6.5 and 7.0 μmol m⁻² which corresponds to 3.9 and 4.2 APTES molecules per nm², respectively. This suggests that silica was present on the surface of the nanoparticles.[53]

3.2. Preparation of CMCS-modified γ-Fe₂O₃ nanoparticles

In order to compare silica-coated γ-F₂O₃ nanoparticles with another type of magnetic particle, CMCS was also selected as a coating of γ-Fe₂O₃ nanoparticles. CMCS was prepared by carboxymethylation. Alkylation can theoretically proceed on N or O atoms with the first reaction being generally preferred due to higher nucleophilicity. However, NMR results confirmed that the oxygen atom on C6 of chitosan was alkylated predominantly,

This journal is © The Royal Society of Chemistry 2011

J. Mater. Chem., 2011, **21**, 7630–7639 | 7633
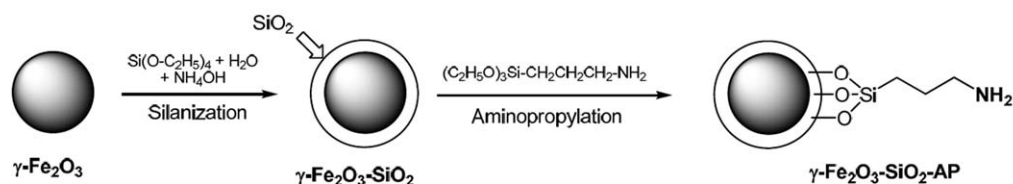
Scheme 1 Silanization of γ-Fe$_2$O$_3$ nanoparticles with TEOS and subsequent modification with APTES.

Table 1 Effect of the APTES concentration in the feed on the surface concentration of APTES on silica-coated γ-Fe$_2$O$_3$ nanoparticles

| APTES in the feed/μmol m^{-2}	Surface concentration of APTES on silica-coated γ-Fe$_2$O$_3$ nanoparticles[a]/μmol m^{-2}
50	3.6
75	6.5
100	7

[a] According to elemental analysis.

while the nitrogen atom only negligibly.[40] CMCS not only ensured the colloidal stability of the resulting nanoparticles, but its advantage consisted in its biodegradability and biocompatibility, which are of key importance for potential applications in human medicine. CMCS was coupled to the γ-Fe$_2$O$_3$ nanoparticles by two approaches: (i) coordination adsorption onto their surface *via* multiple carboxyls and their imino(di)acetate moieties or (ii) covalent attachment to the NH$_2$ groups of γ-Fe$_2$O$_3$-SiO$_2$-AP nanoparticles (Scheme 2). According to TEM micrographs, both the γ-Fe$_2$O$_3$–CMCS and γ-Fe$_2$O$_3$–SiO$_2$-AP–CMCS nanoparticles were almost spherical (Fig. 1(c) and (d)). The mean particle diameter was 9 nm with PDI = 1.17 for γ-Fe$_2$O$_3$–CMCS nanoparticles and 9.3 nm with PDI = 1.15 for γ-Fe$_2$O$_3$–SiO$_2$-AP–CMCS nanoparticles. Even though the CMCS shell was not contrasted in the TEM micrographs of γ-Fe$_2$O$_3$–CMCS nanoparticles, the particles were well separated from each

other, thus suggesting a protective effect of the CMCS shell (Fig. 1(c)). In contrast, γ-Fe$_2$O$_3$–SiO$_2$-AP–CMCS nanoparticles (Fig. 1(d)) resembled the γ-Fe$_2$O$_3$–SiO$_2$-AP nanoparticles (Fig. 1 (b)). The thickness of the shell was also estimated to be 3 nm.

Atomic absorption spectroscopy was used to determine the iron content in neat γ-F$_2$O$_3$, γ-Fe$_2$O$_3$–SiO$_2$-AP, γ-Fe$_2$O$_3$–CMCS and γ-Fe$_2$O$_3$–SiO$_2$-AP–CMCS nanoparticles. While the iron content in neat γ-F$_2$O$_3$ nanoparticles was high (69 wt%), it was lower in γ-Fe$_2$O$_3$–SiO$_2$-AP, γ-Fe$_2$O$_3$–CMCS and γ-Fe$_2$O$_3$–SiO$_2$-AP–CMCS nanoparticles, reaching 44, 48 and 36 wt% of Fe, respectively. This indicated the presence of silica or chitosan shells on the γ-F$_2$O$_3$ cores. The surface modification of γ-F$_2$O$_3$ nanoparticles was also analyzed by elemental analysis. Both the carbon and nitrogen content in γ-Fe$_2$O$_3$–SiO$_2$-AP nanoparticles were lower (2.5 and 0.6 wt%, respectively) than in γ-Fe$_2$O$_3$–SiO$_2$-AP–CMCS nanoparticles (6.3 and 1.3 wt%, respectively). This can be ascribed to the presence of the CMCS layer on the surface of the γ-Fe$_2$O$_3$–SiO$_2$-AP nanoparticles.

3.3. ATR FTIR spectroscopy of γ-Fe$_2$O$_3$–SiO$_2$-AP and CMCS-modified γ-Fe$_2$O$_3$ nanoparticles

The ATR FTIR spectra of surface-modified γ-F$_2$O$_3$ nanoparticles were compared with those of CS, CMCS and neat γ-F$_2$O$_3$ (Fig. 2). The spectrum of CS had characteristic peaks at 1648 cm^{-1} (amide I), 1590 cm^{-1} (N–H bending) and 1080 cm^{-1} (C–O stretching)[40,55]
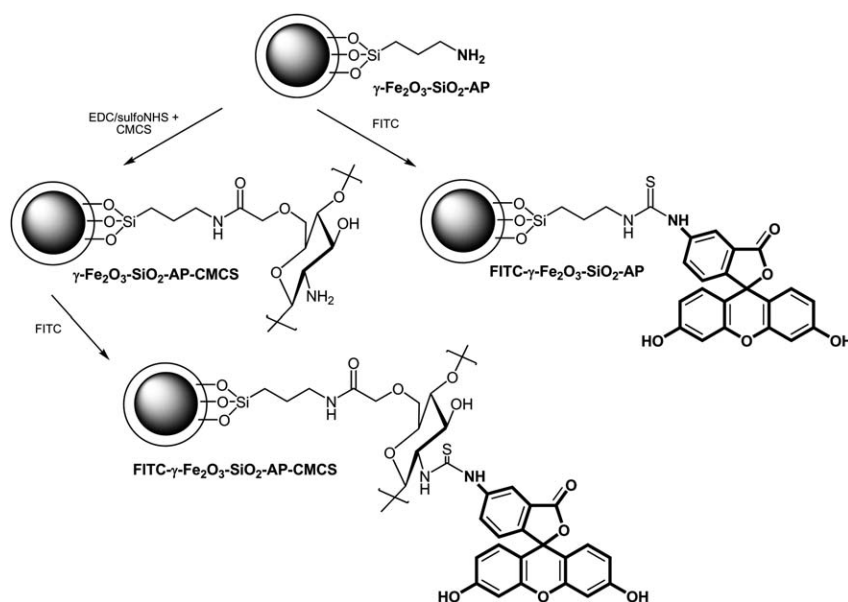
Scheme 2 Labeling of γ-Fe$_2$O$_3$–SiO$_2$-AP and γ-Fe$_2$O$_3$–SiO$_2$-AP–CMCS nanoparticles with FITC.
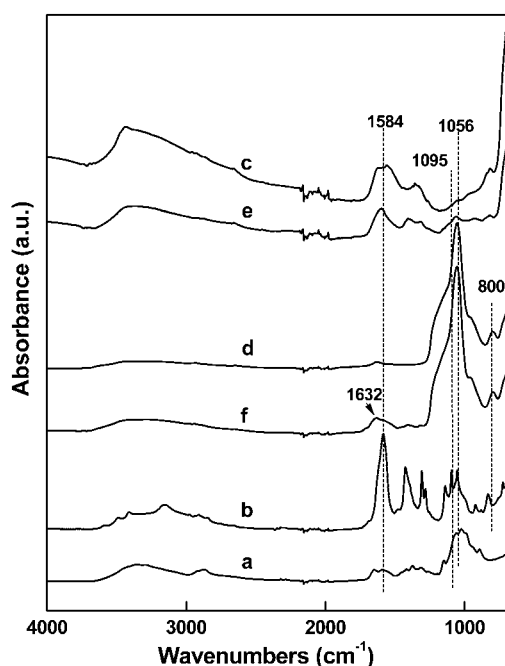
Fig. 2 ATR FTIR spectra of (a) CS, (b) CMCS, (c) neat γ-Fe$_2$O$_3$ nanoparticles, (d) γ-Fe$_2$O$_3$–SiO$_2$-AP nanoparticles, (e) γ-Fe$_2$O$_3$–CMCS nanoparticles and (f) γ-Fe$_2$O$_3$–SiO$_2$-AP–CMCS nanoparticles.

(Fig. 2(a)). In the spectrum of CMCS, peaks at 1095 cm^{-1} attributable to the C–O stretching vibrations and at 1584 cm^{-1} were observed (Fig. 2(b)). The latter peak was intense and broad, which resulted from the overlapping of the peaks of NH$_2$ (1590 cm^{-1}), COOH (1710 cm^{-1}) and COO$^-$ (1598 cm^{-1}) vibrations, which in turn resulted when COOH transferred to COONa.[40] The band with the maximum at 1584 cm^{-1} could also be detected in the spectrum of γ-Fe$_2$O$_3$–CMCS nanoparticles (Fig. 2(e)). The spectra of γ-Fe$_2$O$_3$–SiO$_2$-AP nanoparticles (Fig. 2(d)) and γ-Fe$_2$O$_3$–SiO$_2$-AP–CMCS nanoparticles (Fig. 2(f)) displayed two strong peaks at 1056 cm^{-1} and 800 cm^{-1}, which were assigned to the un-symmetric and symmetric stretching vibrations of Si–O–Si bonding, respectively. This indicated the presence of the silica layer on the surface of the γ-F$_2$O$_3$ nanoparticles. The presence of the primary amino groups (–NH$_2$) in the spectrum of chitosan (Fig. 2(a)) was confirmed by the peak at 1590 cm^{-1}. In the
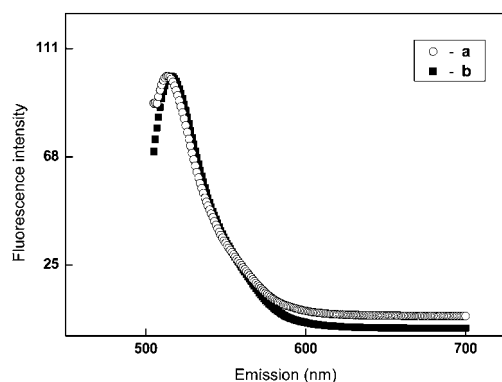
Table 2 r_2 relaxivities of the synthesized nanoparticles

Nanoparticles	r_2 at 0.5 T/s^{-1} mM^{-1}	r_2 at 4.7 T/s^{-1} mM^{-1}
FITC-labeled γ-Fe$_2$O$_3$–SiO$_2$-AP	12.26 $\pm$ 0.05	28.2 $\pm$ 0.9
FITC-labeled γ-Fe$_2$O$_3$–SiO$_2$-AP–CMCS	22.8 $\pm$ 0.2	42.4 $\pm$ 0.4
FITC-labeled γ-Fe$_2$O$_3$–CMCS	28.7 $\pm$ 0.3	47.5 $\pm$ 0.5

spectrum of γ-Fe$_2$O$_3$–SiO$_2$-AP–CMCS nanoparticles, the NH$_2$ peak was overlapped with the peaks of COOH (1710 cm^{-1}) and NHCO (1626 and 1551 cm^{-1}) vibrations, and a new characteristic broad peak at 1632 cm^{-1} was observed (Fig. 2(f)).

3.4. Preparation of fluorescein-modified silica- and CMCS-coated γ-Fe$_2$O$_3$ nanoparticles

The synthesis of the FITC-labeled γ-F$_2$O$_3$ nanoparticles involved three reactions of the FITC isothiocyanate groups with the primary amino groups on the surface of (i) the γ-Fe$_2$O$_3$–SiO$_2$-AP nanoparticles (Scheme 2), (ii) γ-Fe$_2$O$_3$–SiO$_2$-AP–CMCS nano-particles (Scheme 2) and (iii) γ-Fe$_2$O$_3$–CMCS nanoparticles. It is thought that the reactions result in the formation of a stable thiourea linkage between FITC and APTES or CMCS on the nanoparticle surface.

To confirm the attachment of FITC to the γ-F$_2$O$_3$ nano-particles, FITC-labeled γ-Fe$_2$O$_3$–SiO$_2$-AP particles were analyzed by fluorescence spectroscopy. The fluorescence of FITC was measured in a 1% aqueous NH$_4$OH solution. The emission spectra were recorded at an excitation wavelength λ_{ex} = 495 nm over the range of emission wavelengths λ_{em} = 505–700 nm (Fig. 3). As a control, the fluorescence emission spectrum of neat FITC was also recorded for comparison. Both neat FITC and FITC-labeled γ-F$_2$O$_3$ nanoparticles showed the same emission fluorescence peaks at 516 nm and very similar emission spectrum shapes (Fig. 3). No fluorescence was observed in the spectrum of the supernatant after washing of the FITC-labeled γ-F$_2$O$_3$ nanoparticles. This means that the γ-F$_2$O$_3$–SiO$_2$-AP nano-particles were successfully modified with FITC *via* the formation of a stable bond without fluorophore degradation.

Relaxation time measurements revealed lower relaxivities of FITC-labeled γ-Fe$_2$O$_3$–SiO$_2$-AP, γ-Fe$_2$O$_3$–SiO$_2$-AP–CMCS and

Fig. 3 Normalized fluorescence emission spectra of (a) neat FITC (c = 1.4 μM) and (b) FITC-labeled γ-Fe$_2$O$_3$–SiO$_2$-AP nanoparticles (c = 40 mg L^{-1}); λ_{ex} = 495 nm, in 1% NH$_4$OH aqueous solution.
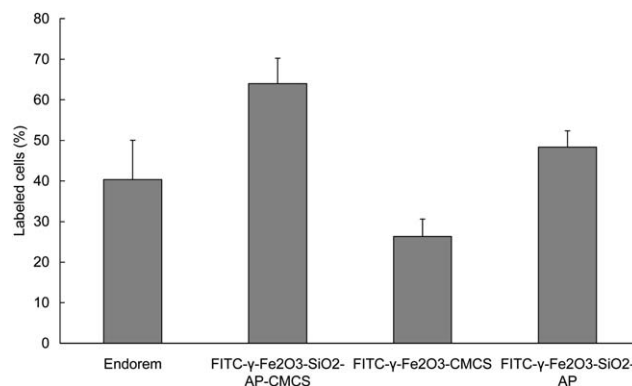

Fig. 4 Labeling efficiency of rMSCs labeled with Endorem® (control), FITC-labeled γ-Fe$_2$O$_3$–SiO$_2$-AP–CMCS nanoparticles, FITC-labeled γ-Fe$_2$O$_3$–CMCS nanoparticles and FITC-labeled γ-Fe$_2$O$_3$–SiO$_2$-AP nanoparticles.

This journal is © The Royal Society of Chemistry 2011

J. Mater. Chem., 2011, **21**, 7630–7639 | 7635

Table 3 R_2 relaxation rates of labeled cell suspensions and estimated iron content per one cell

Cells labeled by	R_2 at 0.5 T/s^{-1} per 10^6 cells in 1 mL	R_2 at 4.7 T/s^{-1} per 10^6 cells in 1 mL	Iron amount/pg per cell
FITC-labeled γ-Fe$_2$O$_3$–SiO$_2$-AP	6.9 ± 0.2	12.7 ± 1.0	28.2 ± 3.2
FITC-labeled γ-Fe$_2$O$_3$–SiO$_2$-AP–CMCS	5.95 ± 0.05	9.57 ± 0.05	13.6 ± 1.0
FITC-labeled γ-Fe$_2$O$_3$–CMCS	2.83 ± 0.03	4.70 ± 0.15	5.5 ± 0.2

γ-Fe$_2$O$_3$–CMCS nanoparticles (Table 2) compared to commercial (carboxy)dextran-coated iron oxides,[56] which may be due to the silica or CMCS coating.

3.5. Cell experiments

Cell labeling with superparamagnetic iron oxides is an increasingly common method for *in vivo* cell monitoring and separation,[57] as the labeled cells can be detected by magnetic resonance imaging. In order to examine the acute toxicity of FITC-labeled γ-Fe$_2$O$_3$–SiO$_2$-AP, FITC-labeled γ-Fe$_2$O$_3$–CMCS and FITC-labeled γ-Fe$_2$O$_3$–SiO$_2$-AP–CMCS nanoparticles, they were incubated with rMSCs for 72 h. Endorem® served as a control. Cell viability was assessed using the trypan blue exclusion test. The viability of rat MSCs labeled with FITC-labeled γ-Fe$_2$O$_3$–SiO$_2$-AP, FITC-labeled γ-Fe$_2$O$_3$–CMCS, FITC-labeled γ-Fe$_2$O$_3$–SiO$_2$-AP–CMCS nanoparticles or with Endorem® was not affected, reaching over 90% and suggesting the biocompatibility (non-toxicity) of the newly developed fluorescent magnetic nanoparticles. Also, the growth of cells in comparison with an unlabeled control was not affected.

As Prussian Blue is a sensitive iron-selective stain, labeling efficiency was assessed by counting Prussian Blue-positive cells.
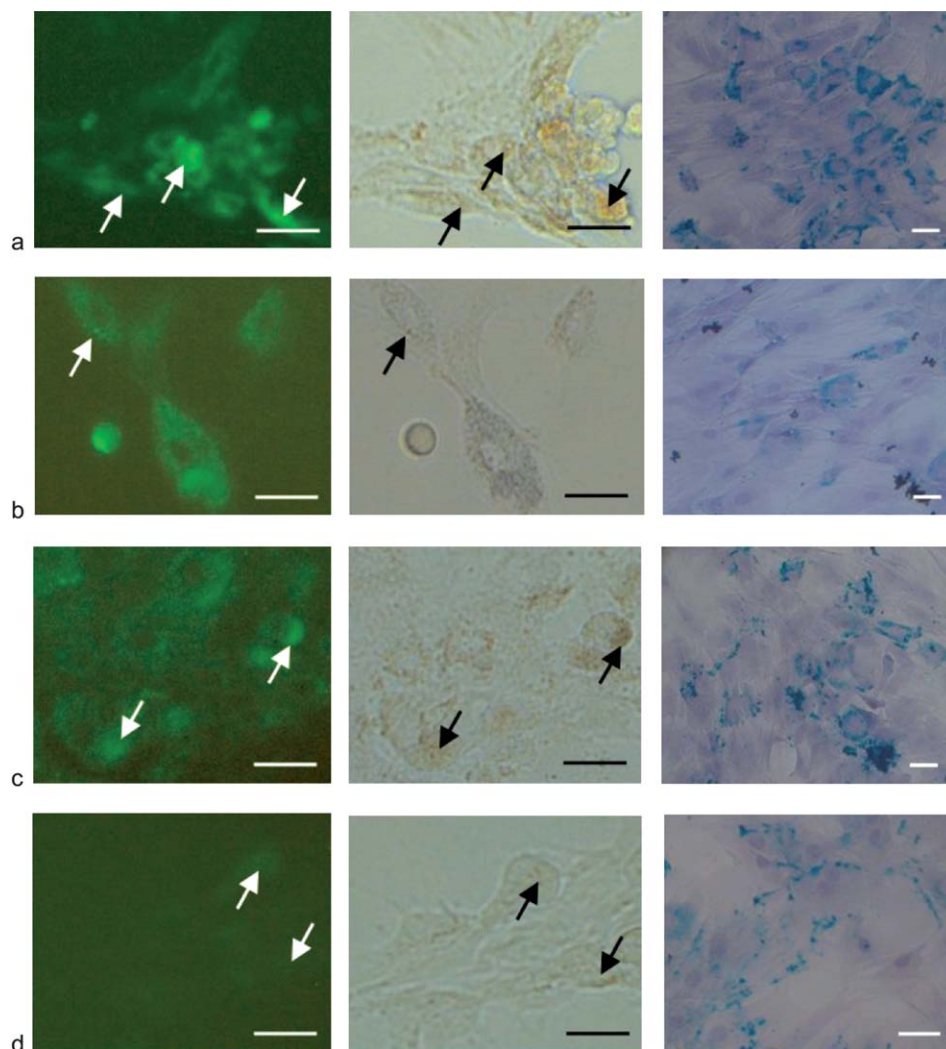

Fig. 5 Left column: fluorescent micrographs of rMSCs labeled with (a) FITC-labeled γ-Fe$_2$O$_3$–SiO$_2$-AP–CMCS nanoparticles, (b) FITC-labeled γ-Fe$_2$O$_3$–CMCS nanoparticles, (c) FITC-labeled γ-Fe$_2$O$_3$–SiO$_2$-AP nanoparticles, and (d) Endorem®. Middle column shows the same cells in an optical field. Arrows mark iron deposits in the cells. Scale bar 50 μm. Right column shows Prussian Blue staining for iron. Scale bar 20 μm.
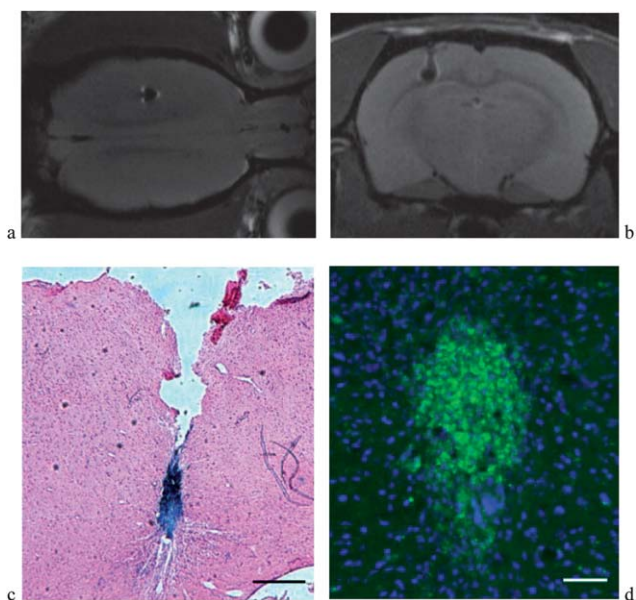
Fig. 6 (a) Coronal and (b) axial magnetic resonance images from a rat brain implanted with 100 000 rMSCs labeled with FITC-labeled γ-Fe$_2$O$_3$–SiO$_2$-AP–CMCS nanoparticles. (c) Cell implant stained for iron using Prussian Blue. Scale bar 0.5 mm. (d) Cell implant visualized in a fluorescent microscope (green), DAPI (blue) stained cell nuclei. Scale bar 50 µm.

All the cells in each optical field (200 $\pm$ 30) were counted and the labeling efficiency was expressed as percentage of Prussian Blue-positive cells. The best results were achieved with FITC-labeled γ-Fe$_2$O$_3$-SiO$_2$-AP–CMCS nanoparticles, where about 64% (64 $\pm$ 3.6) of cells were labeled. FITC-labeled γ-Fe$_2$O$_3$–SiO$_2$-AP nanoparticles labeled 48% (48.3 $\pm$ 4.0) of cells (Fig. 4). This result was comparable with Endorem® labeling of cells, which reached 40% (40.3 $\pm$ 2.0). The worst result was obtained with FITC-labeled γ-Fe$_2$O$_3$–CMCS nanoparticles, where only 26% (26.3 $\pm$ 2.6) of the cells were labeled. Fig. 5 compares the fluorescence intensity. The left and middle columns are from identical cells. Native unstained images of live cells have clear brown deposits from γ-Fe$_2$O$_3$ particles (middle column, black arrows) that clearly correspond to the green fluorescence (white arrows, left column). To distinguish from intrinsic cell autofluorescence, images from Endorem®-labeled cells were included in Fig. 5. Iron oxide deposits showed less fluorescence than FITC-labeled nanoparticles. The right column represents Prussian Blue-stained nanoparticles. The images were taken from the same experiment; however, the cells were not identical. Images in the right column correlate with the labeling efficiency reported in Fig. 4. The differences in labeling efficiency among the different types of nanoparticles were statistically significant (ANOVA on the level $\alpha = 0.01$).

Relaxation measurements reflect the amount of γ-Fe$_2$O$_3$ taken up into the cells. *In vitro* relaxation time measurements confirmed a large amount of iron inside the cells (Table 3). The estimated average amount of iron per cell in the case of FITC-labeled γ-Fe$_2$O$_3$–SiO$_2$-AP was more than two times higher compared to commercially available iron oxide labels,[58] which compensated for the lower relaxivity of the nanoparticles themselves. The differences in iron content in the cells incubated with various types of nanoparticles were statistically significant (ANOVA on the level $\alpha = 0.01$).

3.6. *In vivo* MR imaging

To demonstrate the visualization of labeled cells *in vivo*, 100 000 cells labeled with FITC-labeled γ-Fe$_2$O$_3$–SiO$_2$-AP–CMCS nanoparticles were injected into a rat brain in 3 µL of PBS. The cell implant was nicely visible on MR images as a hypointense spot with excellent contrast against the surrounding tissue (Fig. 6 (a) and (b)). Histology confirmed iron oxide deposits in the cell implant that corresponded to Prussian Blue staining (Fig. 6(c)). The cell implant was also visible when viewed under a fluorescence microscope (Fig. 6(d)).

4. Conclusions

In order to design the dual detection of cells involving imaging by fluorescence and magnetic resonance, two reporters have been included in one particle: a fluorescent dye and a superparamagnetic core. The synthesis procedures to conjugate fluorescent dyes on the magnetic nanoparticle surface required multi-step chemical treatments. In order that the fluorescein-based luminescent component was effectively separated from the maghemite, which is critical in protecting the luminescence from quenching by iron oxide, inert silica, or optionally chitosan layers, was coated on the iron oxide surface. At the same time, this improved the colloidal stability of the particles in the aqueous phase. At feed concentrations $\geq$5 µmol APTES per m^2 of silica-coated γ-Fe$_2$O$_3$ nanoparticles, the iron oxide nanoparticle surface was completely covered with the silica. An organic fluorophore (FITC) was chemically anchored to magnetic γ-Fe$_2$O$_3$–SiO$_2$-AP or γ-Fe$_2$O$_3$–SiO$_2$-AP–CMCS nanoparticles, an approach that is preferred to simple dye adsorption on the γ-Fe$_2$O$_3$–CMCS particles' surface because the latter can easily desorb, thus affecting the response of biological systems to the nanoparticles. FITC-labeled γ-Fe$_2$O$_3$–SiO$_2$-AP–CMCS nanoparticles were best internalized by rMSCs, enabling the visualization of labeled cells *in vivo*. Both CMCS and silica shells were thus necessary to prevent fluorescence quenching of the nanoparticles because FITC was not directly conjugated to the γ-Fe$_2$O$_3$ core but isolated from the environment *via* the shells. The introduction of such cells into the organism, their movement and migration *in vivo* can then be easily monitored by MRI, while optical imaging continuously observes the dynamic intracellular processes of the living cells. Moreover, the fluorescent dye makes quantification after incubation with cells possible. In the future, even trifunctional particles with fluorescence, magnetism and cell recognition can be envisaged.

Bringing together MR and fluorescent molecular imaging, fluorescein-labeled γ-Fe$_2$O$_3$ nanoparticles coated with aminopropylated silica or partly carboxymethylated chitosan can be used for both magnetic and fluorescent labeling, thus providing a powerful tool to study the interaction of the nanoparticles with biological systems. Such labeling offers the possibility of tracking cells by MRI and fluorescent spectroscopic measurements or fluorescent microscopy in cell cultures or even in living organisms.

References

1 B. Perlstein, T. Lublin-Tennenbaum, I. Marom and S. Margel, Synthesis and characterization of functionalized magnetic maghemite nanoparticles with fluorescent probe capabilities for biological applications, *J. Biomed. Mater. Res., Part B*, 2010, **92**, 353–360.

2 S. Laurent, J. L. Bridot, L. V. Elst and R. N. Muller, Magnetic iron oxide nanoparticles for biomedical applications, *Future Med. Chem.*, 2010, **2**, 427–449.

3 C. Corot, P. Robert, J. M. Idée and M. Port, Recent advances in iron oxide nanocrystal technology for medical imaging, *Adv. Drug Delivery Rev.*, 2006, **58**, 1471–1504.

4 C. Sun, J. S. H. Lee and M. Zhang, Magnetic nanoparticles in MR imaging and drug delivery, *Adv. Drug Delivery Rev.*, 2008, **60**, 1252–1265.

5 Z. T. Tsai, J. F. Wang, H. Y. Kuo, C. R. Shen, J. J. Wang and T. C. Yen, *In situ* preparation of high relaxivity iron oxide nanoparticles by coating with chitosan: a potential MRI contrast agent useful for cell tracking, *J. Magn. Magn. Mater.*, 2010, **322**, 208–213.

6 O. Veiseh, J. W. Gunn and M. Zhang, Design and fabrication of magnetic nanoparticles for targeted drug delivery and imaging, *Adv. Drug Delivery Rev.*, 2010, **62**, 284–304.

7 J. H. Lee, K. Lee, S. H. Moon, Y. H. Lee, T. G. Park and J. Cheon, All-in-one target-cell-specific magnetic nanoparticles for simultaneous molecular imaging and siRNA delivery, *Angew. Chem.*, 2009, **48**, 4174–4179.

8 A. Ito, K. Tanaka, H. Honda, S. Abe, H. Yamaguchi and T. Kobayashi, Complete regression of mouse mammary carcinoma with a size greater than 15 mm by frequent repeated hyperthermia using magnetite nanoparticles, *J. Biosci. Bioeng.*, 2003, **96**, 364–369.

9 M. Salloum, R. Ma and L. Zhu, Enhancement in treatment planning for magnetic nanoparticle hyperthermia: optimization of the heat absorption pattern, *Int. J. Hyperthermia*, 2009, **25**, 309–321.

10 I. Šafařík and M. Šafaříková, Magnetic techniques for the isolation and purification of proteins and peptides, *Biomagn. Res. Technol.*, 2004, **2**, 7–34.

11 Z. Zhao, Z. Bian, L. Chen, X. He and Y. Wang, Synthesis and surface-modifications of iron oxide magnetic nanoparticles and applications on separation and analysis, *Prog. Chem.*, 2006, **18**, 1288–1297.

12 A. Kaushik, P. R. Solanki, A. A. Ansari, B. D. Malhotra and S. Ahmad, Iron oxide-chitosan hybrid nanobiocomposite based nucleic acid sensor for pyrethroid detection, *Biochem. Eng. J.*, 2009, **46**, 132–140.

13 A. Quarta, R. Di Corato, L. Manna, A. Ragusa and T. Pellegrino, Fluorescent-magnetic hybrid nanostructures: preparation, properties, and applications in biology, *IEEE Trans. Nanobiosci.*, 2007, **6**, 298–308.

14 Y. Sahoo, A. Goodarzi, M. T. Swihart, T. Y. Ohulchanskyy, N. Kaur, E. P. Furlani and P. N. Prasad, Aqueous ferrofluid of magnetite nanoparticles: fluorescence labeling and magnetophoretic control, *J. Phys. Chem. B*, 2005, **109**, 3879–3885.

15 S. A. Corr, Y. P. Rakovich and Y. K. Gun'Ko, Multifunctional magnetic-fluorescent nanocomposites for biomedical applications, *Nanoscale Res. Lett.*, 2008, **3**, 87–104.

16 P. Howes, M. Green, A. Bowers, D. Parker, G. Varma, M. Kallumadil, M. Hughes, A. Warley, A. Brain and R. Botnar, Magnetic conjugated polymer nanoparticles as bimodal imaging agents, *J. Am. Chem. Soc.*, 2010, **132**, 9833–9842.

17 S. S. Banerjee and D. H. Chen, A multifunctional magnetic nanocarrier bearing fluorescent dye for targeted drug delivery by enhanced two-photon triggered release, *Nanotechnology*, 2009, **20**, 185103.

18 J. Yang, E. K. Lim, H. J. Lee, J. Park, S. C. Lee, K. Lee, H. G. Yoon, J. S. Suh, Y. M. Huh and S. Haam, Fluorescent magnetic nanohybrids as multimodal imaging agents for human epithelial cancer detection, *Biomaterials*, 2008, **29**, 2548–2555.

19 P. Tseng, D. Di Carlo and J. W. Judy, Rapid and dynamic intracellular patterning of cell-internalized magnetic fluorescent nanoparticles, *Nano Lett.*, 2009, **9**, 3053–3059.

20 J. J. Gallagher, R. Tekoriute, J. A. O'Reilly, C. Kerskens, Y. K. Gun'Ko and M. Lynch, Bimodal magnetic-fluorescent nanostructures for biomedical applications, *J. Mater. Chem.*, 2009, **19**, 4081–4084.

21 Y. Ge, Y. Zhang, S. He, F. Nie, G. Teng and N. Gu, Fluorescence modified chitosan-coated magnetic nanoparticles for high-efficient cellular imaging, *Nanoscale Res. Lett.*, 2009, **4**, 287–295.

22 Y. Ichiyanagi, S. Moritake, S. Taira and M. Setou, Functional magnetic nanoparticles for medical application, *J. Magn. Magn. Mater.*, 2007, **310**, 2877–2879.

23 J. H. Lee, B. Schneider, E. K. Jordan, W. Liu and J. A. Frank, Synthesis of complexable fluorescent superparamagnetic iron oxide nanoparticles (fl spions) and cell labeling for clinical application, *Adv. Mater.*, 2008, **20**, 2512–2516.

24 F. Bertorelle, C. Wilhelm, J. Roger, F. Gazeau, C. Menager and V. Cabuil, Fluorescence-modified superparamagnetic nanoparticles: intracellular uptake and use in cellular imaging, *Langmuir*, 2006, **22**, 5385–5391.

25 C. Ren, J. Li, X. Chen, Z. Hu and D. Xue, Preparation and properties of a new multifunctional material composed of superparamagnetic core and rhodamine b doped silica shell, *Nanotechnology*, 2007, **18**, 345604.

26 N. Li, H. Li, D. Chen, H. Liu, F. Tang, Y. Zhang, J. Ren and Y. Li, Preparation and characterization of quantum dots coated magnetic hollow spheres for magnetic fluorescent multimodal imaging and drug delivery, *J. Nanosci. Nanotechnol.*, 2009, **9**, 2540–2545.

27 Z. Y. Ma, D. Dosev, M. Nichkova, S. J. Gee, B. D. Hammock and I. M. Kennedy, Synthesis and bio-functionalization of multifunctional magnetic Fe₃O₄@Y₂O₃:Eu nanocomposites, *J. Mater. Chem.*, 2009, **19**, 4695–4700.

28 I. J. Bruce and T. Sen, Surface modification of magnetic nanoparticles with alkoxysilanes and their application in magnetic bioseparations, *Langmuir*, 2005, **21**, 7029–7035.

29 D. B. Tada, L. L. R. Vono, E. L. Duarte, R. Itri, P. K. Kiyohara, M. S. Baptista and L. M. Rossi, Methylene blue-containing silica-coated magnetic particles: a potential magnetic carrier for photodynamic therapy, *Langmuir*, 2007, **23**, 8194–8199.

30 W. H. Tan, K. M. Wang, X. X. He, X. J. Zhao, T. Drake, L. Wang and R. P. Bagwe, Bionanotechnology based on silica nanoparticles, *Med. Res. Rev.*, 2004, **24**, 621–638.

31 Y. Lu, Y. D. Yin, B. T. Mayers and Y. N. Xia, Modifying the surface properties of superparamagnetic iron oxide nanoparticles through a sol–gel approach, *Nano Lett.*, 2002, **2**, 183–186.

32 X. Hun, Z. Zhang and L. Tiao, Anti-Her-2 monoclonal antibody conjugated polymer fluorescent nanoparticles probe for ovarian cancer imaging, *Anal. Chim. Acta*, 2008, **625**, 201–206.

33 T. Kean and M. Thanou, Biodegradation, biodistribution and toxicity of chitosan, *Adv. Drug Delivery Rev.*, 2010, **62**, 3–11.

34 Y. M. Yang, W. Hu, X. D. Wang and X. S. Gu, The controlling biodegradation of chitosan fibers by *n*-acetylation *in vitro* and *in vivo*, *J. Mater. Sci.: Mater. Med.*, 2007, **18**, 2117–2121.

35 K. A. Janes, P. Calvo and M. J. Alonso, Polysaccharide colloidal particles as delivery systems for macromolecules, *Adv. Drug Delivery Rev.*, 2001, **47**, 83–97.

36 M. N. Kumar, R. A. Muzzarelli, C. Muzzarelli, H. Sashiwa and A. J. Domb, Chitosan chemistry and pharmaceutical perspectives, *Chem. Rev.*, 2004, **104**, 6017–6084.

37 T. Kean and M. Thanou. Chitin and Chitosan—Sources, Production and Medical Applications, in *Desk Reference of Natural Polymers, their Sources, Chemistry and Applications*, ed. P. A. Williams and R. Arshady, Kentus Books, London, 2009, pp. 327–361.

38 A. P. Zhu, N. Fang, M. B. Chan-Park and V. Chan, Interaction between *O*-carboxymethylchitosan and dipalmitoyl-*sn-glycero-3*-phosphocholine bilayer, *Biomaterials*, 2005, **26**, 6873–6879.

39 A. Zhu, M. B. Chan-Park, S. Dai and L. Li, The aggregation behavior of *O*-carboxymethylchitosan in dilute aqueous solution, *Colloids Surf., B*, 2005, **43**, 143–149.

7638 | *J. Mater. Chem.*, 2011, **21**, 7630–7639

This journal is © The Royal Society of Chemistry 2011

40 X. G. Chen and H. J. Park, Chemical characteristics of *O*-carboxymethyl chitosans related to the preparation conditions, *Carbohydr. Polym.*, 2003, **53**, 355–359.

41 J. Magali, A. Hernandez, A. Maurras, K. Puget, M. Amblard, J. Martinez and G. Subra, *N*-terminus FITC labeling of peptides on solid support: the truth behind the spacer, *Tetrahedron Lett.*, 2009, **50**, 260–263.

42 S. Vira, E. Mekhedov, G. Humphrey and P. S. Blank, Fluorescent-labeled antibodies: balancing functionality and degree of labeling, *Anal. Biochem.*, 2010, **402**, 146–150.

43 N. Dias, J. F. Goossens, B. Baldeyrou, A. Lansiaux, P. Colson, A. Di Salvo, J. Bernal, A. Turnbull, D. Mincher and C. Baily, Oxoazabenzo[*de*]anthracenes conjugated to amino acids: synthesis and evaluation as DNA-binding antitumor agents, *Bioconjugate Chem.*, 2005, **16**, 949–958.

44 K. Pachmann, K. Reinecke, B. Emmerich and E. Thiel, Highly fluorochrome labeled gene probes for quantitative tracing of RNA in individual cells by *in situ* hybridization, *Bioconjugate Chem.*, 1991, **2**, 19–25.

45 M. Hruby, C. Konak and K. Ulbrich, Polymeric micellar pH-sensitive drug delivery system for doxorubicin, *J. Controlled Release*, 2005, **103**, 137–148.

46 Y. Bae, N. Nishiyama, S. Fukushima, H. Koyama, M. Yasuhiro and K. Kataoka, Preparation and biological characterization of polymeric micelle drug carriers with intracellular pH-triggered drug release property: tumor permeability, controlled subcellular drug distribution, and enhanced *in vivo* antitumor efficacy, *Bioconjugate Chem.*, 2005, **16**, 122–130.

47 M. Babič, D. Horák, P. Jendelová, K. Glogarová, V. Herynek, M. Trchová, K. Likavčanová, M. Hájek and E. Syková, Poly(*N,N*-dimethylacrylamide)-coated maghemite nanoparticles for stem cell labeling, *Bioconjugate Chem.*, 2009, **20**, 283–294.

48 Z. L. Shi, K. G. Neoh, E. T. Kang, B. Shuter, S. C. Wang, C. Poh and W. Wan, (Carboxymethyl)chitosan-modified superparamagnetic iron oxide nanoparticles for magnetic resonance imaging of stem cells, *ACS Appl. Mater. Interfaces*, 2009, **1**, 328–335.

49 S. Čampelj, D. Makovec and M. Drofenik, Functionalization of magnetic nanoparticles with 3-aminopropyl silane, *J. Magn. Magn. Mater.*, 2009, **321**, 1346–1350.

50 O. Hiraku and M. Yoshiharu, Biodegradation and distribution of water-soluble chitosan in mice, *Biomaterials*, 1999, **20**, 175–182.

51 S. A. Azizi, D. Stokes, B. J. Augelli, C. DiGirolamo and D. J. Prockop, Engraftment and migration of human bone marrow stromal cells implanted in the brains of albino rats. Similarities to astrocyte grafts, *Proc. Natl. Acad. Sci. U. S. A.*, 1998, **95**, 3908–3913.

52 K. A. Carvalho, C. C. Cury, L. Oliveira, R. I. Cattaned, M. Malvezzi, J. C. Francisco, A. Pachalok, M. Olandoski, J. R. Faria-Neto and L. C. Guarita-Souza, Evaluation of bone marrow mesenchymal stem cell standard cryopreservation procedure efficiency, *Transplant. Proc.*, 2008, **40**, 839–841.

53 R. K. Iler, *The Chemistry of Silica*, Wiley, New York, 1979.

54 M. Yamaura, R. L. Camilo, L. C. Sampaio, M. A. Macêdo, M. Nakamurad and H. E. Toma, Preparation and characterization of (3-aminopropyl)triethoxysilane-coated magnetite nanoparticles, *J. Magn. Magn. Mater.*, 2004, **279**, 210–217.

55 J. Brugnerotto, J. Lizardi, F. M. Goycoolea, W. ArguÈelles-Monal, J. DesbrieÁres and M. Rinaudo, An infrared investigation in relation with chitin and chitosan characterization, *Polymer*, 2001, **42**, 3569–3580.

56 M. Babič, D. Horák, P. Jendelová, K. Glogarová, V. Herynek, M. Trchová, K. Likavčanová, M. Hájek and E. Syková, Poly(*N,N*-dimethylacrylamide)-coated maghemite nanoparticles for stem cell labeling, *Bioconjugate Chem.*, 2009, **20**, 283–294.

57 O. Olsvik, T. Popovic, E. Skjerve, K. S. Cudjoe, E. Hornes, J. Ugelstad and M. Uhlen, Magnetic separation techniques in diagnostic microbiology, *Clin. Microbiol. Rev.*, 1994, **7**, 43–54.

58 P. Jendelová, V. Herynek, J. DeCroos, K. Glogarová, B. Andersson, M. Hájek and E. Syková, Imaging the fate of implanted bone marrow stromal cells labeled with superparamagnetic nanoparticles, *Magn. Reson. Med.*, 2003, **50**, 767–776.

This journal is © The Royal Society of Chemistry 2011

J. Mater. Chem., 2011, **21**, 7630–7639 | 7639